Research Square

Preprints are preliminary reports that have not undergone peer review.
They should not be considered conclusive, used to inform clinical practice,
or referenced by the media as validated information.

Constraint-based mathematical model analysis reveals glycogen and cellulose storage competition during conversion of CO2 to hyaluronic acid in Chlorella vulgaris

Pratik Ramchandra Chaudhari
National Institute of Technology Rourkela
Alisha Zaffar
National Institute of Technology Rourkela
Muhil Raj Prabhakar
National Institute of Technology Rourkela
Balasubramanian Paramasivan
National Institute of Technology Rourkela
Bikash Chandra Maharaj
bikash.maharaj@gmail.com

National Institute of Technology Rourkela

Research Article

Keywords:

Posted Date: March 19th, 2026

DOI: https://doi.org/10.21203/rs.3.rs-9064306/v1

License: This work is licensed under a Creative Commons Attribution 4.0 International License.
Read Full License

Additional Declarations: No competing interests reported.

Constraint-based mathematical model analysis reveals glycogen and cellulose storage competition during conversion of CO2 to hyaluronic acid in *Chlorella vulgaris*

Pratik Ramchandra Chaudhari, Alisha Zaffar, Muhil Raj Prabhakar, Balasubramanian Paramasivan, Bikash Chandra Maharaj*

Department of Biotechnology and Medical Engineering, National Institute of Technology Rourkela, Odisha -769008, India

*Corresponding author:
Dr. Bikash Chandra Maharaj
Department of Biotechnology and Medical Engineering
National Institute of Technology Rourkela
Sector 1, Rourkela, Sundergarh
Odisha, India
PIN - 769008
Email: bikash.maharaj@gmail.com; maharajb@nitrkl.ac.in,
Phone: 9337683769/7873479777

Abstract

Hyaluronic acid (HA) is a biopolymer with a wide range of biomedical and industrial applications. Conventionally, it is manufactured from rooster comb and fermentation of *Streptococcus zooepidemicus*. In this work, we explore hyaluronic acid production under phototrophic conditions using a reduced-scale, constraint-based in silico microalgal model comprising 216 reactions, 144 metabolites, and 318 genes, reconstructing a microalgal system. In model validation, verify stoichiometric consistency, phototrophic conditions, and constraints, and also check for leaks in reaction flux. Single limiter analysis shows the HA production steadily increases with photon from (0.05 to – 0.31 mmol gDW^{-1} h^{-1}), and CO_2 (0.1 to 1 mmol gDW^{-1} h^{-1}), uptake, indicating strictly resource-limited biosynthesis. Trade-off analysis between biomass-HA under phototrophic growth, where the wild-type state produced HA = 0.26 mmol gDW^{-1} h^{-1} with biomass flux ~3.88–4.00 mmol gDW^{-1} h^{-1}. Enforcing storage allocation activated glycogen and cellulose sinks, diverting carbon away from HA and decreasing HA to ~0.15 mmol gDW^{-1} h^{-1}, along with reduced growth. Pareto and weighted-sum optimization revealed a steep, non-smooth front, indicating discrete switching between growth and HA-dominated metabolic states. Knockout of the competing storage reactions redirected carbon toward HA biosynthesis, recovering HA to ~0.26 mmol gDW^{-1} h^{-1} without decreasing biomass growth.

Introduction

Hyaluronic acid is a linear biopolymer entailing two crucial repeating polysaccharide units of D-glucuronic acid and N-acetyl-glucosamine (Palenčárová et al., 2025a). Its unique physiochemical properties, such as high viscosity, retention quality, and biocompatibility, have aided its application in the fields of pharmaceuticals, orthopaedics, and regenerative medicine (Sundaram et al., 2025). HA has been used for the treatment of osteoarthritis, ophthalmic surgery, dermal fillers, drug delivery systems, and tissue engineering scaffolds (Saadh et al., 2025; Shang et al., 2024). Globally, the HA market has shown an annual exponential growth of 8.3 billion USD (Salih et al., 2024). Furthermore, the market is expected to rise in future due to increasing cosmetic procedures, age-related health issues and innovations in biomaterial science. Previous scientific literature has harvested HA from animal tissues, such as bovine trachea, rooster combs, and umbilical cords (Palenčárová et al., 2025b). Despite high molecular weight HA production, extraction procedures are often tedious, protein- and nucleic acid-contaminated, and carry risks of immunogenicity and disease transmission (Grabowski et al., 2025). Moreover, batch-to-batch inconsistency limits

their industrial scalability and acceptability by the regulatory authorities. Therefore, heterotrophic microbial fermentation with Streptococcus species has emerged as the predominant industrial process, as it offers greater titres and scalability (Orth et al., 2010). However, conventional fermentation is based on crop sugars whose production and processing create upstream GHG emissions, countering the environmental benefits of bioproducts (Wróbel-Jędrzejewska et al., 2024). Additionally, aseptic conditions and air supply make the overall process uneconomical (Li et al., 2024; Zhang et al., 2023). Hence, the utilisation of phototrophic microorganisms such as cyanobacteria and microalgae has been recognised as a potential host for next-generation production.

Phototrophic microorganisms fix atmospheric CO_2 using light energy to drive metabolism by the Calvin- Benson- Bassham (CBB) cycle, which fixes, enabling the direct conversion of CO_2 and H_2O into target metabolites (Liu & Yu, 2025). HA production through phototrophic microorganisms reduces the carbon footprint by utilizing atmospheric CO_2 as a carbon source, does not require arable land or potable water for cultivation, and is compatible with industrial flue gas CO_2 streams with minimum risk of contamination from heterotrophic systems (Son et al., 2025). Recent developments in metabolic engineering have reported heterologous expression of HA biosynthetic pathways, PmHAS or SeHasA, in cyanobacterial hosts, that concludes detectable accumulation of HA under phototrophic growth conditions (Son et al., 2025; Wei et al., 2024). Although titres are still less than those in heterotrophic systems (typically in the 14-80 mg/L range), previous research confirms it as a carbon-neutral HA biosynthesis (L. Zhang et al., 2019). Low titres are primarily attributed to limitations in precursor supply, energy and redox partitioning, and carbon partitioning in phototrophic cells. Unlike heterotrophs, phototrophs must balance HA biosynthesis with photoautotrophic energy production, CO_2 fixation, and competing carbon sinks such as glycogen or photorespiration, leading to complex intracellular flux patterns (Yang et al., 2024). Genome-scale metabolic models (GSMs) and Flux Balance Analysis (FBA) provide robust platforms for engineering and analysing such metabolic trade-offs.

GSMs accurately represent the biochemical reaction networks within an organism, enabling the prediction of feasible steady-state flux distributions under genetic and environmental constraints (Carter et al., 2024). FBA was successfully employed with heterotrophic hosts, such as *E. coli* and *S. cerevisiae*, to elucidate pathway bottlenecks,

optimise precursor supply, and simulate gene knockouts to enhance HA production (Heirendt et al., 2019). In phototrophic systems, FBA facilitates the quantitative analysis of light-dependent metabolism, CO_2 fixation, and polymer biosynthesis, thereby guiding metabolic engineering strategies, regardless of the iterative experimental steps involved (Scott et al., 2023).

Initially, dynamic flux balance analysis was employed to describe and predict diauxic growth behaviour in E coli. After a decade, dFBA was applied for lipid production under the autotrophic, mixotrophic and heterotrophic conditions in Chlorella sp. FC2 (Muthuraj et al., 2013). For this method, the light and dark conditions were maintained in the experiment and the model. Hybrid models that incorporate artificial intelligence and machine learning, as well as FBA, integrate the results of both approaches to enhance metabolic predictions by understanding nonlinear regulation and dynamics in Synechococcus sp. PCC 7002, Escherichia coli and Pseudomonas putida . Recent studies reveal that artificial intelligence approaches for simulating metabolic dynamics using approximate FBA models are scalable and extremely fast (Song et al., 2025).

Chlorella vulgaris is a fast-growing and robust green microalgae with a high protein composition and the ability to grow in photoautotrophic, heterotrophic, and mixotrophic modes, making this organism highly desirable for biotechnological applications due to its diverse biochemical composition and metabolic flexibility. . There have been effective studies proving the feasibility of the organism in fixing CO_2, as well as in the scale-up process, in both photobioreactors and open systems. There has been more emphasis on systems biology and flux balance analysis for carbon distribution and optimisation in the past few years. HA production from different algae, like cyanobacterium *Synechococcus elongatus* PCC 7942 and cyanobacterium *Synechococcus* sp. PCC 7002 (Son et al., 2025; L. Zhang et al., 2019) .This work focuses on the sustainable production of hyaluronic acid (HA) using the microalgae Chlorella vulgaris.

Despite the broad biological importance of microalgae, HA biosynthesis has not been systematically studied in *Chlorella vulgaris.* Moreover, nutrient limitations, precursor bottlenecks, and carbon-light co-regulation remain unexplored in *C. vulgaris*. Understanding these limitations is key to establishing microalgae as suitable platforms for photosynthetic HA production. Hence, in the present study, a structurally consistent

metabolic model of *Chlorella vulgaris* was reconstructed, and a comprehensive suite of constraint-based analysis was applied to understand HA biosynthetic capacity under photoautotrophic conditions to (i) assess the stoichiometric consistency, structural completeness, and mass-balance properties of the reconstructed microalgal metabolic network, which consisted of 144 metabolites and 216 reactions; (ii) quantify hyaluronic acid production under a spectrum of environmental constraints through single limiter robustness sweeps for CO_2 and photon, identifying limited regimes; (iii) apply ε-constraint multi-objective analysis to characterize growth–product trade-offs amongst biomass, glycogen storage, and HA production (iv) Gene knockout analysis in comparative scenario framework illustrating carbon allocation in no-forcing, storage-enriched WT, and storage-synthase KO states and (v) shadow price analysis of metabolites. The integration of phototrophic physiology, HA biosynthesis, metabolic flux modelling, and advanced bioprocess engineering focuses on developing a large-scale and sustainable platform for HA production from CO_2.

1. Material and method

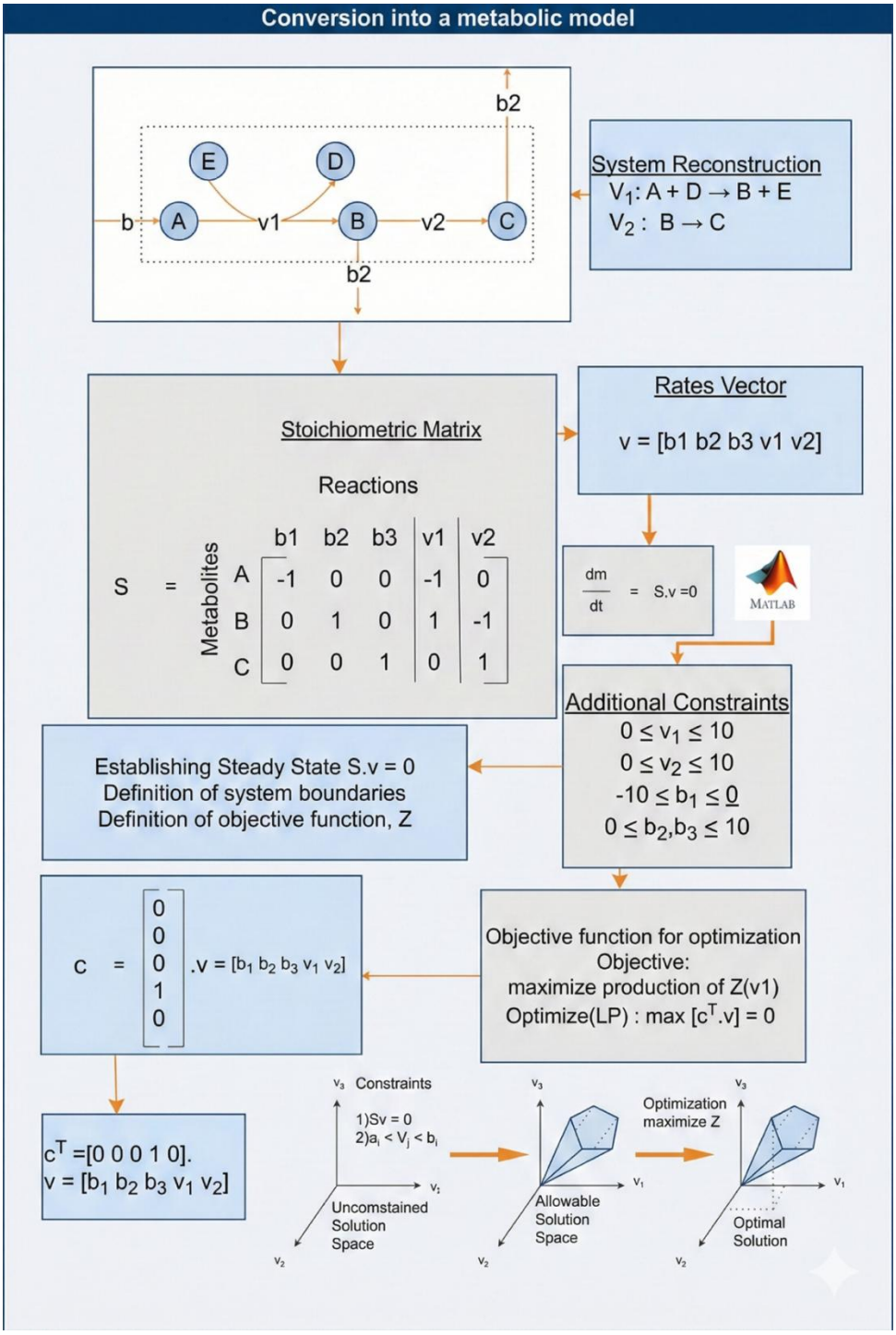


Figure 1: Schematic Overview of the FBA Methodology

1.1 Data Collection and Model Formulation

The genome-scale metabolic model of *Chlorella vulgaris iCZ843*, comprising 843 genes, 2,294 reactions, and 1,770 metabolites, was previously developed in the

literature (Zuñiga et al., 2016)and is used as the reference model in this study. The constructed reduced-scale metabolic model (microalgae61200) specific to the biosynthesis of HA features two cellular compartments: the cytoplasm and the extracellular region. The reason behind this approach was to facilitate the central carbon metabolism and HA-related reaction pathways without computational difficulties. Moreover, the model was validated through structural and functional consistency checks to ensure mathematical correctness and biological relevance. Stoichiometric and flux feasibility analyses were used to confirm balanced network with a valid solution space.

1.2 Flux Balance Analysis

Figure 1 shows that Biochemical and genetic data were systematically gathered from various biological databases, including KEGG, NCBI, UniProt, and Phytozome to reconstruct the reduced-scale model using FBA. The gathered information included metabolic reactions, reaction names, stoichiometric parameters, metabolite names, gene relations, reaction orientations, and physiologically relevant constraints. Absence of locus tag descriptions for *Chlorella vulgaris* in the database restricted reconstruction of the whole process; hence, gene locus tags identified in *Chlamydomonas reinhardtii* were used as an alternative in this study as both eukaryotic microalgae belong to the green algae group, characterized by a conserved carbon metabolism. However, all biochemical reactions were formally described with correct stoichiometry and orientation in accordance to the conventional reaction formula, where negative and positive sign indicate consumed substrate and produced product, respectively.

The reduced-scale model can be mathematically described as a stoichiometric matrix *S*. The stoichiometric matrix *S* was constructed according to well-curated biochemical pathways, where *m* represents the number of metabolites and *n* represents the number of reactions. Reactions in these models can be categorized into internal, transport, and exchange reactions (Becker et al., 2007b).

The reconstructed metabolic network model comprises metabolites, reactions, bounds on fluxes, and an objective function. The reversibility of reactions was considered carefully based on biological evidence. Irreversible reactions constraints values within a range between 0 and 1000 mmol gDW^{-1} h^{-1}, while reversible reactions between the values of −1000 and 1000 mmol gDW^{-1} h^{-1}. Exchange reaction rules for nutrient uptake

and secretion, such as photon uptake (EX_Photon), carbon dioxide uptake (EX_CO_2), and nitrate uptake (EX_NO_3), were fixed using gene sensitivity analysis and model feasibility. All reaction rules were reviewed for mass balance, charge balance, and redox equality to remove infeasible cycles by checking stoichiometric equality.

With the assumption of steady state, the concentration of the metabolite in the cell remains constant, and the system follows the mass balance equation **(Eq.1)** (Orth et al., 2010):

$$S.v = 0 \qquad \textbf{Eq. 1}$$

where *S(i,j)* is the stoichiometric coefficient of metabolite *i* in reaction *j*, and *v* is the reaction flux.

If *S(i, j)* < 0 metabolite *i* reacts in reaction *j*

If *S(i, j)* > 0, metabolite *i* is produced by reaction *j*

If *S(i,j)* = 0, then metabolite *i* does not involve reaction *j*.

Each flux in the reactions v_j had constraints given by lower and upper boundaries **(Eq.2)** (Orth et al., 2010)

$$v_j^{min} \leq v_j \leq v_j^{max} \qquad \textbf{Eq. 2}$$

v_j is the flux of reaction *j*, representing its reaction rate in the FBA model.

1.2.1 Single limiter Robustness analysis

Objective function optimization is required in flux balance analysis to define the cellular metabolic goal. In this study, maximizing hyaluronic acid secretion was used to examine carbon allocation and growth production trade-offs.

The optimization problem was set up as a linear programming problem: **(Eq. 3)** (Orth et al., 2010)

$$maximize \quad Z = c^T.v \qquad \textbf{Eq. 3}$$

Z is the objective function value, and c is the weight vector. Although biomass production is most widely used as an optimization function in modelling, the focus of this study was the production of Hyaluronic Acid; hence, the secretion reaction of Hyaluronic Acid (EX_HA(e)) was set as 1 in the objective function, with all other

reaction values set to zero. With this formulation, it is guaranteed that HA production during optimization is maximized. **(Eq.4)** (Orth et al., 2010)

$$v_j = 0 \qquad \textbf{Eq. 4}$$

v_j is the flux of reaction *j*, representing its reaction rate in the FBA model.

1.2.2 Multi-objective optimization

Flux Variability Analysis (FVA) was performed to calculate the minimum and maximum possible flux in each reaction, satisfying the optimal level of HA production. FVA helps in understanding the flexibility of the network, alternative paths, and reaction robustness at the optimal solution point. Furthermore, trade-offs between growth and product synthesis were evaluated through multi-objective optimization employing the ε-constraint and weighted sum approach. In constrained (ε-constraint) method, the production of HA was forced as a minimum share of its theoretical maximum, represented in **Eq. 5** (Mahadevan & Schilling, 2003)

$$v_{HA} = \alpha . v_{HA}^{max} \qquad \textbf{Eq. 5}$$

Where α is a fraction of the maximum HA flux enforced.

The weighted sum approach optimized the biomass growth rate and HA production rate together **(Eq. 6)** (Burgard & Maranas, 2001)

$$\max Z = w_1 . v_{Biomass} + w_2 . v_{HA} \qquad \textbf{Eq. 6}$$

where w_1 and w_2 are weighting factors that determine the emphasis on growth relative to production.

1.3 Competitive Pathway Analyses.

The different scenarios to study the influence of different pathways on the production of hyaluronic acid are discussed in the subsequent sections:

2.3.1 Baseline wild-type (WT) FBA (unforced allocation)

No enforcing scenario applies the optimize function with linear programming having hyaluronic acid production as the only objective function **Eq. 7** (Orth et al., 2010)

$$maximize\ Z = v_{HA} \qquad \textbf{Eq. 7}$$

These conditions did not have any additional constraints specific to forcing carbon fluxes into storage reactions, such as glycogen or cellulose synthesis, whereas non-zero flux values were present in the synthesis of biomass and HA. The linear program solver favours the direction of flux towards achieving the objective function, which means metabolic flux is driven more towards producing HA than towards other low-priority reactions.

2.3.2 WT with enforced storage carbon allocation (flux-enforced glycogen/cellulose)

To simulate the increased storage of assimilated carbon in the cell, specific constraints on carbon partitioning were incorporated into the wild-type model. The assimilated carbon flux into biomass and storage was distributed in a fixed proportion as follows: **Eq.8-10** (Burgard & Maranas, 2001)

$$v_{biomass} \geq \alpha . v_{biomass}^{max} \quad \textbf{Eq. 8}$$

$$v_{Gly} \geq \beta . v_{Gly}^{max} \quad \textbf{Eq. 9}$$

$$v_{Cel} \geq \gamma . v_{Cell}^{max} \quad \textbf{Eq. 10}$$

These constraints activate storage competing pathways, thus redirecting carbon fluxes towards synthesis of glycogen and cellulose. Biomass and HA have same precursor, so flux of both reaction is declined.

2.3.3 Storage-pathway knockout mutant (competing pathway deletion for HA rerouting.

In the gene knockout scenario, there were no forcing constraints on biomass production, but knockout the competitive pathway such as glycogen and cellulose. **Eq. 11-12** (Feist et al., 2010)

$$v_{Gly} = 0 \quad \textbf{Eq. 11}$$

$$v_{cel} = 0 \quad \textbf{Eq. 12}$$

Hence, carbon flux is diverted towards objective function (HA). These gene knockouts show that deletion of competitive pathway increase the flux towards objective function.

1.4 Shadow Price Analysis

Shadow price analysis was performed to identify metabolites whose presence limits biomass or hyaluronic acid production. It also helps to quantify the changes and understand the effect on the optimal objective value when constraints are applied. The analysis helps confirm the model's accurate response to nutrient and energy limitations, thereby identifying metabolic bottlenecks in HA synthesis.

The FBA problem is formulated as per Eq. 1, 2, and 3. Upon optimization, the dual variables associated with the mass-balance constraints Eq.1 were extracted from the solver output as the shadow-price vector (λ), obtained in the COBRA Toolbox as sol.y. Each shadow price λ_i corresponds to metabolite *i* and represents the marginal change in the optimal objective value with respect to a unit relaxation of its steady-state constraint: **Eq. 13** (Ho, 2000)

$$\lambda_i = \frac{\partial Z}{\partial b_i} \qquad \textbf{Eq. 13}$$

where Z is the optimal objective value and b_i denotes the right-hand side of the metabolite balance equation.

Non-zero shadow prices identified objective-limiting metabolites, and their consistent behaviour across HA objectives and photon-limited conditions validated the model's HA-focused predictions.

2. Results and discussion

3.1 Structural and stoichiometric validation of the metabolic model

This constructed model (microalgae61200) contained 216 reactions, 144 metabolites, and 318 genes. Also, it contains central pathways such as core carbon fixation, central metabolism, UDP sugar biosynthesis, and the HA Production pathway. Before conducting quantitative simulations, the model undergoes a detailed validation protocol to analyse its structural and functional integrity. Structural analysis and validation are summarised in **Table 1**. Structural analysis revealed that the reduced FBA network (144 metabolites, 216 reactions) is mathematically well-specified and suitable for FBA simulations. The stoichiometric matrix contained no invalid entries (NaN/Inf = 0), and the model had no empty reaction columns or metabolite rows, confirming that all reactions/metabolites are represented in the mass-balance system ($S.v = 0$) without

breaking stoichiometric consistency. Flux bounds were also internally consistent (bad lb/ub = 0; lb > ub = 0). These suggest that infeasibility does not arise from improper constraint formulation, and that the model satisfies established model validation criteria for constraint-based reconstructions.

Rank nullity analysis (rank(S) = 141; nullity in reaction space = 75) indicates substantial feasible degrees of freedom in flux space, meaning the model can support multiple alternative steady-state flux distributions under the same environment, an expected property of genome-scale and reduced metabolic networks. The metabolite-space nullity = 3 suggests limited linear dependency relations, consistent with a compact, curated reconstruction. Such rank/nullity reporting is commonly used to characterize structural flexibility prior to optimization.

Model-based gap indicators identified 21 dead-end metabolites and 22 degree-1 reactions, reflecting metabolites with only production or only consumption connectivity and reactions with minimal network coupling. In reconstruction protocols, in constraint-based modelling, these features serve as gap-analysis indicators, distinguishing intentional boundary metabolites from structural gaps due to missing transport or pathway coverage."

A notable result is the high number of blocked reactions (107), indicating that these reactions cannot carry flux under any steady-state condition, given the current network connectivity and bounds. Reconstruction guidelines explicitly note that blocked reactions are typically caused by dead-end metabolites or missing links and are routinely used to guide curation and gap filling. In practice, they may remain in reduced models when the corresponding biology is outside the scope. COBRA Toolbox workflows treat blocked-reaction and dead-end network statistics as primary measures of structural quality.

Stoichiometric consistency checks detected one stoichiometrically inconsistent reaction, implying one reaction violates mass conservation (often due to incorrect stoichiometric coefficients, missing substrates/products such as H_2O/H^+, or an improperly defined pseudo-reaction). Because the inconsistency count is low (1 of 216), the network is largely mass-balanced; however, this reaction should be corrected (e.g., if deliberately defined as a pseudo/exchange-like formulation). Ensuring

stoichiometric consistency is a standard requirement in reconstruction protocols and is directly emphasized in modern model validation.

Finally, boundary structure appears correct the model contains 21 exchange reactions, and importantly none have zero stoichiometry columns (0), confirming exchanges are implemented as proper boundary fluxes rather than empty placeholders. Well-formed exchanges are essential for defining environmental conditions and a consistent model result.

Moreover, structural analysis of the model confirms that the reconstructed metabolic network is both computationally robust and stoichiometrically consistent, thereby providing a stable and well-posed platform to support constraint-based simulations and metabolic engineering analysis. Comparable structural indicators have been widely used to benchmark the metabolic network fidelity of *Streptococcus zooepidemicus*, *Escherichia coli*, and *Synechococcus* strains engineered for HA production (Son et al., 2025) . These preliminary steps of model validation are essential, as structural gaps often result in misleading flux predictions within large-scale constraint-based models (Scott et al., 2023). Leak tests under fully closed uptake conditions yielded infeasible linear programs, confirming the absence of artificial internal cycles (Kumar S & Bhatt, 2025). Collectively, these results verified that the model is structurally sound and well-defined for subsequent Flux Balance Analysis (FBA) and robustness analysis.

Table 1. Structural and stoichiometric validation metrics for the metabolic model

Property	**Value**
mets (m)	144
rxns (n)	216
rank (S)	141
nullity (rxn space)	75
nullity (met space)	3
NaN in S	0
Inf in S	0
Zero rxns columns	0
Zero metabolite rows	0
Bad lb entries	0

Bad ub entries	0
lb>ub count	0
Dead-end metabolites (count)	21
Degree-1reactions (count)	22
Blocked reactions (count)	107
Stoichio-inconsistent reactions (count)	1
Missing formula mets (count)	0
Missing charge mets (count)	NaN
Exchange reactions (count)	21
EX with zero stoichiometry column (count)	0

3.2 Robustness of metabolic system behaviour under single nutrient-limitation constraints

3.2.1 Effect of Photon uptake

Figure 2 illustrates the impact of photon availability on hyaluronic acid (HA) production. An increase in HA production correlates directly with increased photon intake. Photons support HA production and enable the photosynthesis of carbon and energy assimilation, suggesting that HA is a significant product of the photosynthetic process. The increase in HA production becomes moderate as the photon uptake rates reach higher levels (>180 mmol $gDW^{-1}h^{-1}$), indicating secondary metabolic limitations on HA flux before the full saturation of the photon supply. Thus, photon supply is concluded to be a crucial factor in determining HA production when only one factor is limiting, and enhancing the light supply will enable a significant increase in HA production productivity (Höper et al., 2024). The model predicts that photon limitation plays the dominant role at low uptake levels and continues to constrain the HA flux even under moderate illumination, implying that ATP and NADPH availability to be critical determinants of polymer synthesis. The findings are consistent with previous reported studies in cyanobacteria, that confirmed that HA biosynthesis to be coupled with the efficiency of photosynthetic and carbon-fixation machinery (Case & Atsumi, 2016; Son et al., 2025).

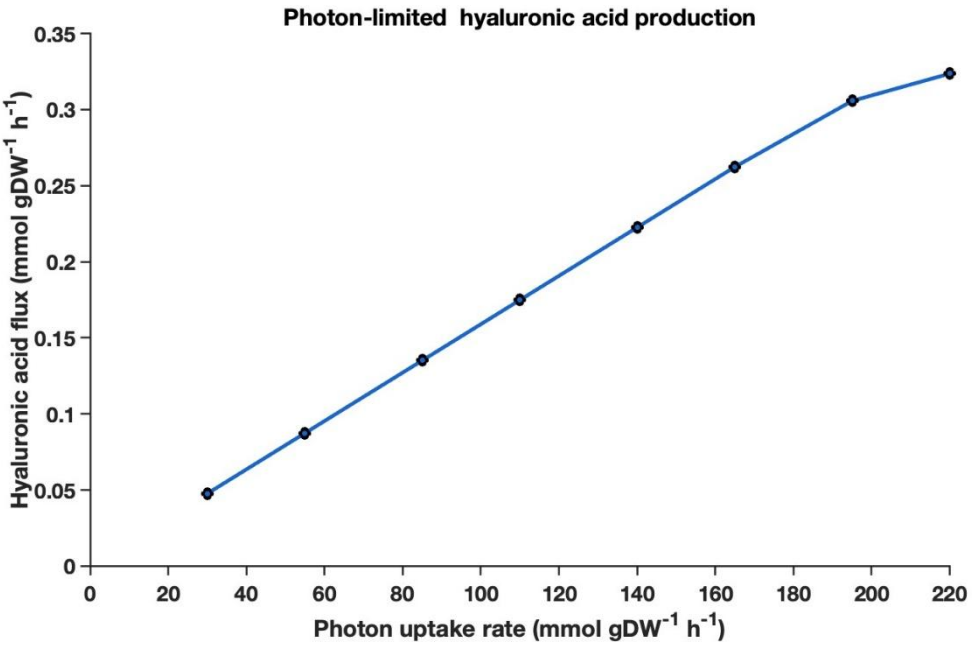


Figure 2: Effect of Photon uptake on hyaluronic acid (HA) flux under single-limiter conditions

3.2.2 Effect of CO_2 uptake

The influence of CO_2 uptake on HA biosynthesis using single limiter robustness sweep is depicted in **Figure 3**. The analysis shows a monotonic increase in HA flux as the respective uptake bounds were incrementally relaxed, suggesting the absence of metabolic saturation under the simulated range. Progressive relaxation of the lower bound from 0 to –4.38 mmol gDW^{-1} h^{-1} resulted in a steady rise in HA flux from approximately 0 to 0.32 mmol gDW^{-1} h^{-1} under a strongly constrained limited condition. The role of CO_2 availability is similar to the limitation behaviour in photoautotrophic and heterotrophic HA-producing organisms (Son et al., 2025). Carbon precursor limitation in HA production studies emphasises its role in Calvin cycle, UDP-sugar metabolism, and hexosamine intermediates. Similar carbon-limited flux responses are observed in engineered microbial strains where HA titre correlates with CO_2 enrichment, carbon-feed optimisation, or CO_2 capture enhancements (Lee et al., 2025; Yu et al., 2023; L. Zhang et al., 2019). The convergence of our findings with those of previous studies suggests that the importance of carbon supplementation to enhance HA biosynthesis in chlorella vulgaris.

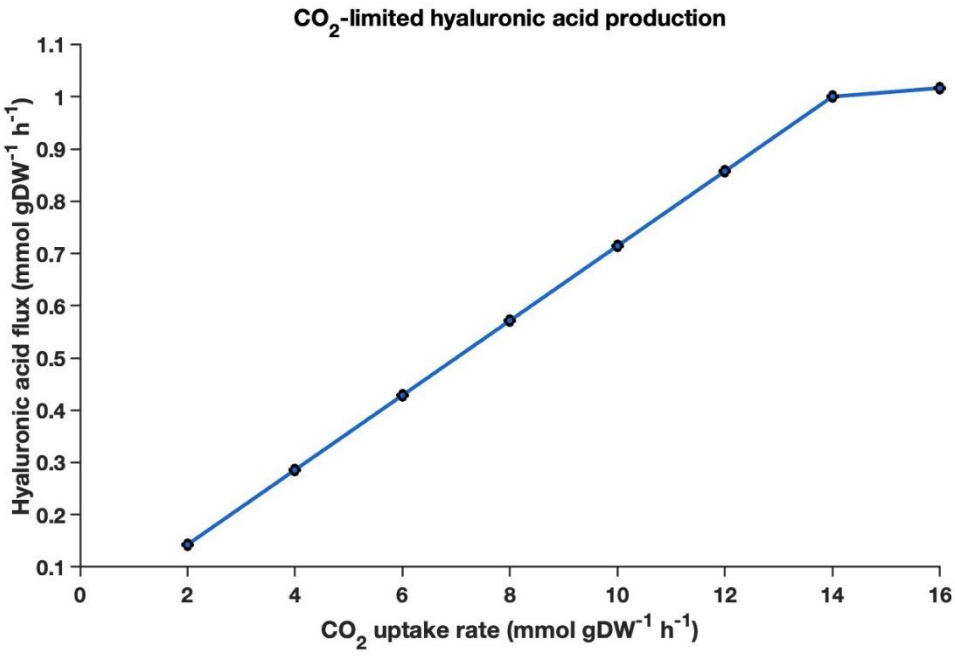


Figure 3: Effect of CO_2 uptake on hyaluronic acid (HA) flux under single limiter conditions

3.3 Multi-objective optimisation elucidates the biomass–HA trade-off under constrained environments

3.3.1 Scenario 1: Impact of enforced multi-objective constraints on metabolic flux allocation

The relationship between biomass and the Hyaluronic Acid (HA) production is illustrated in **Figure 4**. Biomass production was observed to be ~4.02 mmol gDW^{-1} h^{-1} with negligible HA synthesis in the absence of enforcement ($\alpha = 0$). Consequently, when enforcement was increased ($\alpha \approx 0.2$), an increment in HA production (0.06 mmol gDW^{-1} h^{-1}) without any negative impact on biomass yield (~4.01 mmol gDW^{-1} h^{-1}) was observed. Similar enhancement in HA (0.13 mmol gDW^{-1} h^{-1}) and biomass yield (4.00 mmol gDW^{-1} h^{-1}) when the enforcement is further increased to $\alpha \approx 0.4$. However, further increase of enforcement ($\alpha \approx 0.6$) results in decreased production of biomass (~3.95 mmol gDW^{-1} h^{-1}) and an increase HA yield (~0.18 mmol gDW^{-1} h^{-1}). Moreover, a similar pattern of biomass (~3.88–3.90 mmol gDW^{-1} h^{-1}) and HA (~0.26 mmol gDW^{-1} h^{-1}) production was observed at a higher enforcement level of $\alpha \approx 0.8$. Thus, suggesting that the metabolic costs associated with high levels of HA production become increasingly limiting. (Griesemer & Navid, 2023).

Figure 5 depicts the relationship between biomass and HA production in Pareto frontier. The maximum level of biomass observed at the growth optimality extreme was 4.02 mmol $gDW^{-1}h^{-1}$, with HA production is >0.05 mmol $gDW^{-1}h^{-1}$. Furthermore, an increase of HA production from ≥0.05 to ~ 0.12-0.13 mmol $gDW^{-1}h^{-1}$, results in decrease of associated biomass yield between 3.97-3.98 mmol $gDW^{-1}h^{-1}$, representing efficacious trade-off zone. Similarly, with further increment in HA production (0.26 mmol $gDW^{-1}h^{-1}$), drop in biomass production was observed (decreasing to 3.88 mmol $gDW^{-1}h^{-1}$). An increase in HA flux with decrease in biomass at higher levels of enforcement in the multi-objective plot of the compromise curve (Pareto trade-off), is due to carbon/energy allocation across competing biological objectives (Griesemer & Navid, 2023). Thus confirming that elevated levels of HA compromise competitiveness for growth in chlorella vulgaris.

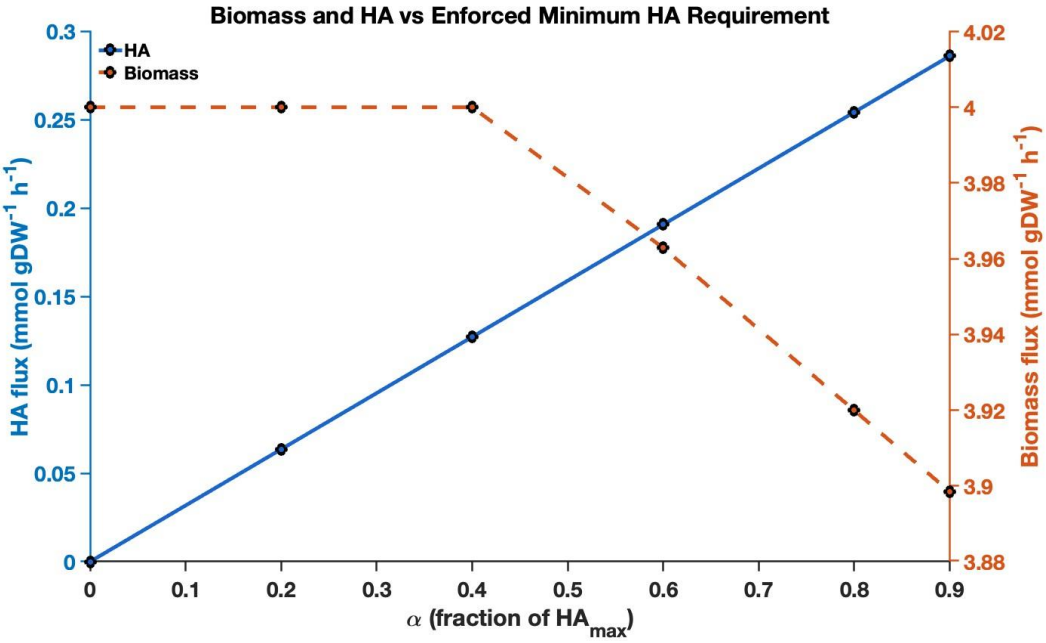


Figure 4: Biomass and HA flux responses to enforce minimum requirements (ε-constraint formulation).

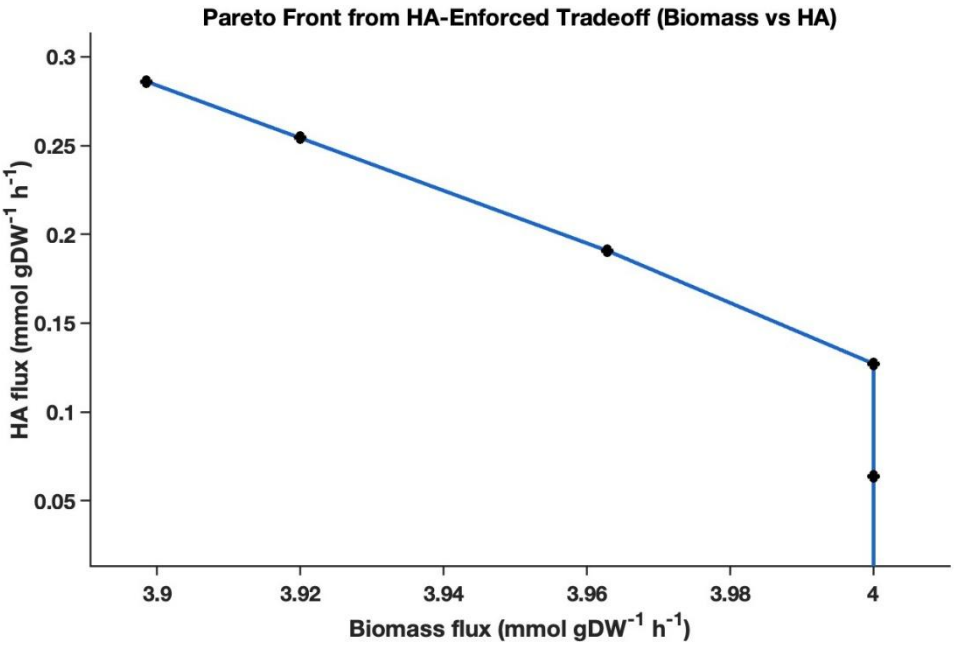


Figure 5: Pareto Optimization of Biomass and HA

3.3.2 Scenario 2: Weighted-sum multi-objective optimisation of competing metabolic objectives

Weighted-sum multi-objective optimisation **Figure 6** revealed a systematic and quantitative trade-off between biomass formation and hyaluronic acid (HA) production under the enforced metabolic constraints. When a higher weight was allocated to biomass, the model converged to near-maximal growth states, with biomass fluxes in the range of approximately 3.87–3.95 mmol gDW^{-1} h^{-1}. Under these conditions, the corresponding HA flux decreased sharply and frequently collapsed to ~0 mmol gDW^{-1} h^{-1}, indicating that HA synthesis is not growth-coupled in the present metabolic configuration. This behaviour reflects preferential routing of carbon, energy, and cofactors toward biomass-associated processes when growth is prioritised (Lin et al., 2025) .

In contrast, increasing the relative weight assigned to HA production, marked an increase in HA flux to approximately 0.28–0.31 mmol gDW^{-1} h^{-1}, accompanied by a reduction in biomass flux to ~3.60–3.70 mmol gDW^{-1} h^{-1}. Substantially, this reduction corresponds to only a ~5–8% decrease in growth, yet enables large gain in HA production. These results indicate that HA synthesis requires extensive flux redirection toward UDP-sugar and polymer biosynthetic pathways, even at near-optimal growth. Importantly, the optimisation exhibited a discontinuous Pareto front in which both

objectives were simultaneously maximised, underscoring the intrinsic trade-off between growth and HA production.

The weighted-sum solutions also exhibited non-smooth transitions in objective values across neighbouring weight combinations, with pronounced switching between HA-producing and HA-inactive states. This phenomenon is characteristic of linear programming-based metabolic models and reflects the presence of alternative optimal flux distributions within the feasible solution space. Similar discrete metabolic switching has been reported in multi-objective flux balance analysis studies, where small changes in objective weighting select fundamentally different Pareto-optimal states rather than a continuous spectrum of solutions. Such behaviour is therefore not an artefact but an expected outcome of competing objectives embedded within a constrained metabolic network (Marler & Arora, 2010) .

The Pareto front derived from the weighted-sum solutions further supports the existence of a strong trade-off. Pareto-optimal results shows biomass range of approximately 3.60–3.95 mmol gDW^{-1} h^{-1}, while HA flux varies from ~0 to ~0.30 mmol gDW^{-1} h^{-1}. At near-maximal growth, HA production is consistently negligible, whereas elevated HA flux is observed only under reduced growth conditions. Pareto-optimal cannot simultaneously achieved biomass flux above ~3.8 mmol gDW^{-1} h^{-1} and HA flux above ~0.1 mmol gDW^{-1} h^{-1}, which confirms there is no growth-coupled HA synthesis. The Pareto front exhibits a steep, non-linear slope, indicating high sensitivity of HA production to changes in growth.

Overall, the co-optimised effect of both weighted-sum and Pareto analyses demonstrates that HA production competes strongly with growth for shared metabolic resources, including carbon skeletons, energy, and activated sugar nucleotides. The observed trade-off structure and discrete switching behaviour are consistent with previously reported multi-objective FBA studies, validating that the present model reflects biologically relevant growth–production trade-offs. Collectively, the results demonstrate that achieving higher HA flux necessitates constraint-based reformulation to reshape the objective trade-off space in favour of HA production, beyond growth-coupled optimisation.

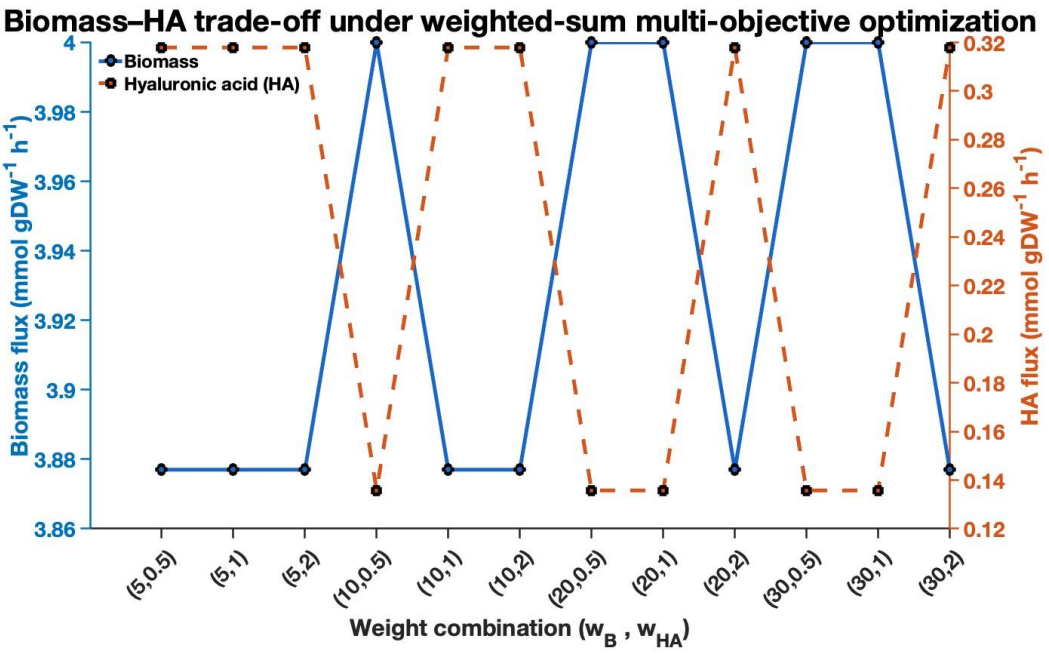


Figure 6: Weight sum Analysis of Biomass-HA co-optimization

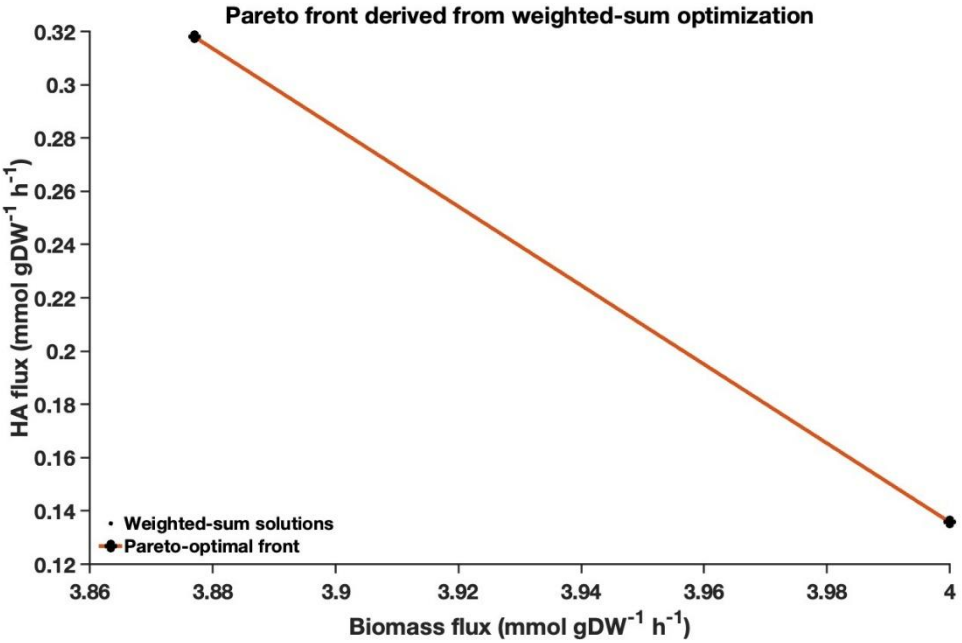


Figure 7: Pareto front analysis of biomass-HA trade off

3.4 Gene Knockout Analysis

A metabolic pathway of HA **Figure 8a** is illustrated as a reconstructed phototrophic pathway for Carbon dioxide sequestration driven by hyaluronic acid biosynthesis, which emphasises major energy and carbon sources useful for HA precursor availability. Photon supply explicitly comes from the exchange reaction of photons

(EX_Photon), which supplies photons to the intracellular pathway for further energy production reactions, such as the Light reaction. This reaction utilises photons and forms byproducts like ATP and NADPH, which serve as energy sources that support downstream carbon assimilation and anabolic metabolism. Additionally, light-driven pathways integrate with exchange reactions to export and transport photosynthetic byproducts. Specifically, oxygen exchange (EX_O2) facilitates the export of oxygen to the extracellular environment after its formation from the light reaction, whereas proton exchange (EX_H) exports protons to the extracellular environment during phototrophic HA synthesis.

Carbon entry into central metabolism occurs via the CO_2 exchange reaction (EX_CO2), enabling transfer of carbon dioxide from the extracellular boundary to intracellular compartments. Then, carbon assimilation is carried out through the Calvin cycle to generate core sugar phosphate intermediates that serve as the central distribution nodes. Among these, Fructose-6-phosphate (F6P) is the primary carbon source of carbon fixation and represents a key precursor for the linkage of the primary metabolism pathway for HA biosynthesis. A reversible isomerisation reaction of Fructose 6-phosphate (F6P) and Glucose-6-phosphate (G6P) enhances metabolic flexibility for both metabolites, creating biosynthetic branches for sugar nucleotides, which are required for HA polymer formation.

In the G6P-derived branch, carbon is routed toward nucleotide sugar activation through conversion of G6P to glucose-1-phosphate (G1P) by phosphoglucomutase, followed by addition of Uridine Triphosphate (UTP) for synthesis of Uridine Diphosphate glucose (UDP-Gluc) catalysed by UDP-glucose pyrophosphorylase (GtaB). UDP-Gluc is subsequently oxidised to UDP-glucuronic acid (UDP-GlucUA) via UDP-glucose dehydrogenase (TuaD), generating the glucuronic acid donor required for HA assembly. In parallel, the F6P-derived branch channels flux into amino sugar metabolism, such as Glucosamine-6-phosphate synthase (GlmS), which initiates the synthesis of glucosamine-6-phosphate (GlucN6P), later isomerization of (GlucN6P) to glucosamine-1-phosphate (GlucN1P) converted through the N-acetylglucosamine-1-phosphate uridyltransferase (GlmU_iso) followed by UDP-N-acetylglucosamine-1-phsophate (UDP-GlucNAc1P) formation through Glucosamine-1-phosphate N-acetyltransferase (GlmU_acetyl_tranferase) and finally second essential nucleotide formation UDP-N-acetylglucosamine (UDP-GlucNAcP) by N-acetylglucosamine-1-

phosphate uridyltransferase (GlmU_uridyl_tranferase representing the second essential sugar nucleotide precursor. The convergence of these two activated pools UDP-GlucUA and UDP-GlucNAc—defines the terminal HA biosynthetic step, where HA synthase (SeHasA) polymerizes the repeating disaccharide units to form HA. Product secretion is represented explicitly by the HA exchange/export reaction (EX_HA), enabling extracellular release and direct quantification of HA productivity under constraint-based optimization.

A key insight from the schematic is the presence of strong competitive carbon sinks that reduce net precursor flow into HA biosynthesis. Specifically, the G1P pool can be diverted toward ADP-glucose formation and glycogen biosynthesis, while UDP-Gluc can alternatively feed cellulose, both of which compete with UDP-GlucUA formation for shared upstream metabolites. This competition establishes a mechanistic basis for the gene knockout framework presented in the subsequent analysis (Figure 9) by disrupting glycogen and cellulose-associated flux demands. The model predicts that a larger fraction of fixed carbon can be redirected toward HA precursor synthesis, thereby improving HA formation without requiring increased photon or CO_2 uptake.

Figure 8b illustrates how each metabolic constraint and genetic configuration, relative to the production of HA, behaves in terms of output product rate as a function of time. Three scenarios considered for the study are discussed in details in subsequent sections.

A) Scenario I: Baseline wild-type (WT) FBA (unforced allocation)

Gene knockout analysis was performed under a non-enforced flux allocation model, where hyaluronic acid export (EX_HA(e)) was optimized independently, and without an additional constraints on competing storage pathways. In the optimized regime, the model achieved a maximum HA flux of 0.26 mmol gDW^{-1} h^{-1}, accompanied by a biomass flux of 3.905 mmol gDW^{-1} h^{-1}. This indicates that, although the competing storage pathways for glycogen and cellulose remained structurally present in the network, they did not carry flux in the optimal solution. This behaviour is consistent with standard flux balance analysis, which utilises a linear programming solver. This prioritises routing flux exclusively through pathways that directly contribute to the defined objective function, while alternative pathways with no contribution to the objective remain inactive unless explicitly enforced.

The lack of flux through glycogen and cellulose pathways indicates that, under HA-maximising conditions, carbon partitioning toward storage does not improve the objective value relative to HA synthesis or biomass formation. Consequently, carbon flux is preferentially channelled through central metabolism and HA biosynthetic reactions, yielding the same maximal HA flux as observed in the wild-type model. Notably, the maximum HA flux did not exceed 0.26 mmol gDW^{-1} h^{-1}, demonstrating that gene knockouts, exclusively without additional environmental constraints, do not exceed the wild-type optimum. This result is consistent with established constraint-based modelling theory, which predicts that gene deletions typically flux the feasibility region and cannot improve an objective unless competing pathways are actively constrained . Thus, these results validate the wild-type HA flux as an upper bound under the given conditions and justify the need for enforced multi-objective or pathway-constraining strategies to further enhance HA production.

B) Scenario II: WT with enforced storage carbon allocation (flux-enforced glycogen/cellulose)

In the storage-enriched wild-type scenario, explicit carbon allocation constraints were introduced to activate competitive storage pathways for glycogen and cellulose while maintaining the overall wild-type model. Carbon partitioning was enforced such that 40% of carbon was allocated to biomass formation ($\alpha = 0.4$), while the remaining fraction was equally allocated to glycogen ($\beta = 0.2$) and cellulose ($\gamma = 0.2$) synthesis (Mori et al., 2016). This constraint formulation was designed to represent physiological conditions in which excess carbon is diverted into storage compounds, rather than being exclusively allocated to support growth or product formation.

Within the model, glycogen biosynthesis is represented by two parallel reactions (GlgA1 and GlgA2), whereas cellulose synthesis occurs through a single reaction (CesA). Upon enforcement of the allocation constraints, both storage pathways became active and carried measurable fluxes of approximately 0.122 mmol gDW^{-1} h^{-1}, confirming successful activation of these competing sinks. The comparable flux levels across glycogen and cellulose further indicate that the applied constraints effectively balanced carbon distribution between the two storage polymers, despite variation in pathway structure.

The activation of storage metabolism had a pronounced impact on growth and hyaluronic acid (HA) production. After the activation of the storage pathway, it has an impact on biomass and HA, as indicated by the simultaneous decline in their fluxes, 1.6 mmol gDW^{-1} h^{-1} & ~0.15 mmol gDW^{-1} h^{-1}, respectively, relative to the wild-type, non-enforced scenario. This reduction reflects direct competition between Biomass, HA biosynthesis, and storage pathways, as they all draw from common central metabolic precursors for shared carbon and energy resources. Overall, these results qualitatively demonstrate a clear metabolic trade-off between growth-associated storage processes and heterologous product formation, highlighting the cost of diverting carbon toward storage under enforced allocation regimes.

C) scenario III: Storage-pathway knockout mutant (competing pathway deletion for HA rerouting.

Deletion of competitive carbon storage pathways, specifically glycogen and cellulose biosynthesis, was performed to remove major metabolic sinks that compete with hyaluronic acid (HA) production. As shown in **Figure 9**, five distinct gene knockout (KO) combinations targeting these pathways were evaluated (L. Zhang et al., 2019). Throughout all KO designs, the model consistently achieved an HA flux of approximately 0.26 mmol gDW^{-1} h^{-1} alongside a biomass flux of ~3.9 mmol gDW^{-1} h^{-1}, values that are comparable to the wild-type optimum. This result indicates that removal of storage pathways improves intracellular carbon availability without compromising growth, thereby stabilising the optimal carbon flux distribution toward HA synthesis.

From a constraint-based modelling perspective, gene knockouts reduce the dimensionality of the feasible flux space by eliminating alternative pathways that otherwise dissipate carbon flux. In this case, deletion of glycogen and cellulose pathways effectively removed competitive sinks, allowing carbon to be preferentially channelled through central metabolism and the HA biosynthetic route (Son et al., 2025). However, despite this redirection, the maximum achievable HA flux did not exceed the wild-type optimum. This behaviour reflects a fundamental property of flux balance analysis, discussed when the objective function has already reached its global maximum under given environmental and uptake constraints; further pathway deletions cannot increase the optimal value unless additional constraints are relaxed or enforced.

The observation that HA flux remains unchanged after gene knockout is therefore not indicative of model limitation, but rather confirms theoretical expectations. Numerous metabolic engineering studies have demonstrated that deletion of competing pathways often stabilises target product flux and preserves biomass yield, rather than increasing production beyond intrinsic network limits. Consequently, the agreement between wild-type and KO flux values in this study validates both the internal consistency of the model and the appropriateness of the applied knockout strategy. These results further suggest that additional interventions such as enforced flux allocation, precursor overproduction, or uptake relaxation are required to shift the HA production threshold beyond the wild-type maximum.

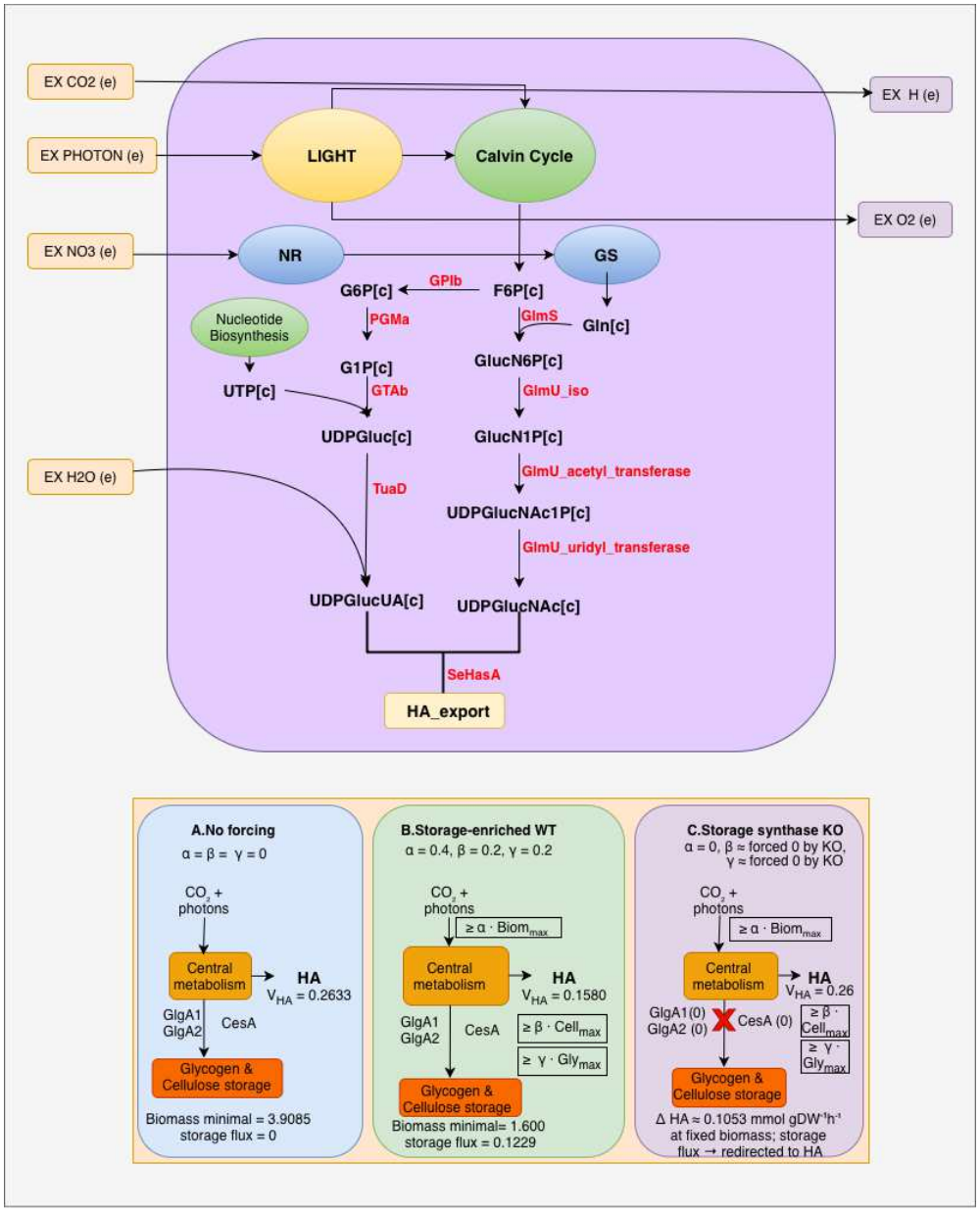


Fig. 8(a): Schematic overview of light-driven CO_2 assimilation toward hyaluronic acid biosynthesis and Fig. 8(b) Comparison of three FBA scenarios showing how biomass forcing, storage enrichment, and storage knockouts affect HA production

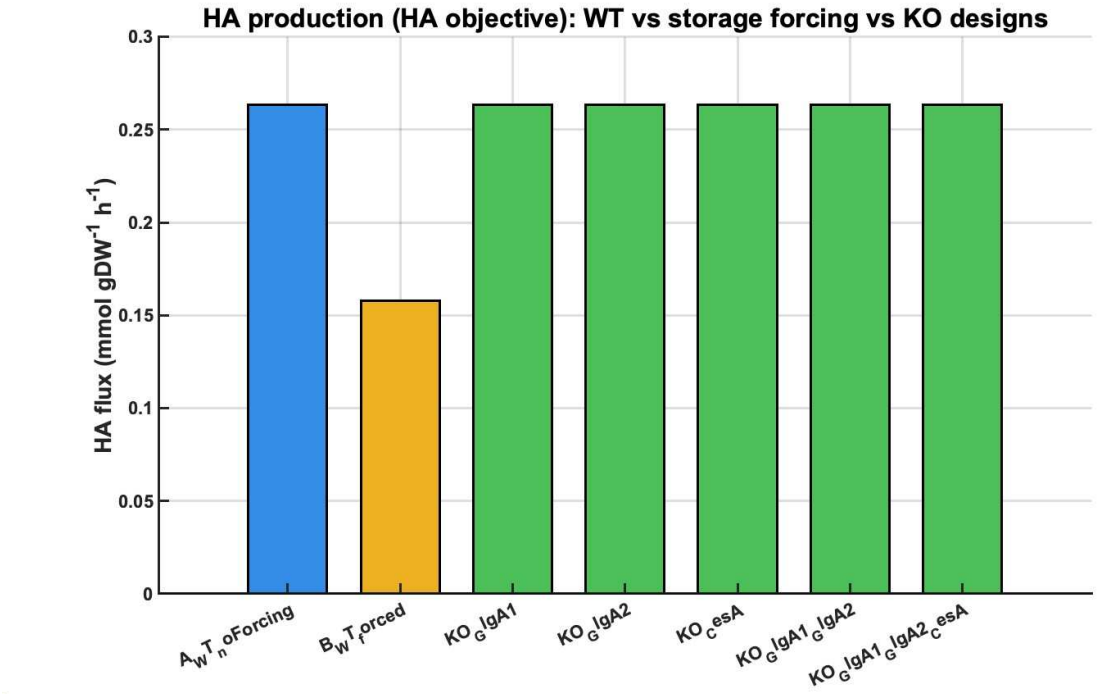


Fig 9: HA flux comparison across WT, storage-forced, and knockout designs

3.5 Shadow Price Analysis

Table 2: Shadow price analysis of intracellular metabolites under HA-maximizing conditions

Metabolites	Shadow Price
G6P[c]	0.398093
F6P[c]	0.398093
FBP[c]	0.398093
GAP[c]	0.199046
DHAP[c]	0.199046
NAD[c]	-0.03158
BPG[c]	0.167461
3PG[c]	0.167461
PEP[c]	0.167461

Pyr[c]	0.167461
COA[c]	-0.13588
OA[c]	-0.16269
AKG[c]	-0.16269
SCOA[c]	-2.11283
FAD[c]	-0.03158
Fum[c]	-0.13111
Mal[c]	-0.13111
GOX[c]	0.169051
NADP[c]	-0.03317
PGL[c]	0.364918
R5P[c]	0.331744
Ro5P[c]	0.331744
X5P[c]	0.331744
SH7P[c]	0.464441
E4P[c]	0.265395
O2[c]	-0.06317
FA[c]	1.642127
NL[c]	5.158601
UTP[c]	-0.13111
G1P[c]	0.398093
UDPGluc[c]	0.266985
UDP[c]	-0.13111
Ser[c]	0.298569
NH4[c]	0.131108
Gln[c]	0.131108
CAP[c]	0.131108
ace[c]	0.135877
THF[c]	0.033174
Gly[c]	0.331744
H2S[c]	0.033174
Cys[c]	0.331744

Ala[c]	0.330154
3HPyr[c]	0.135877
PRPP[c]	0.331744
Tyr[c]	0.129518
AICAR[c]	-0.16269
Photon[c]	0.00159
GMP[c]	-0.03158
UMP[c]	-0.13111
GTP[c]	-0.03158
dTMP[c]	-0.13111
dTTP[c]	-0.13111
Chl[c]	-0.47377
SAHC[c]	0.033174
H2O2[c]	-0.03158
PS[c]	0.398093
DNA[c]	-0.02491
RNA[c]	-0.0347
UDPGlucUA[c]	0.203815
GlucN6P[c]	0.5292
GlucN1P[c]	0.5292
UDPGlucNAc[c]	0.533969
HA[c]	1
HA[e]	1
GlucNAc1P[c]	0.665077
Photon[e]	0.00159
3PG[c]	0.165872
RUBP[c]	0.331744
NH4[c]	0.13110
O2[e]	-0.06317

As shown in **Table 2**, Shadow-price analysis (dual variables of the steady-state constraints) provides a quantitative measure of sensitivity to marginal changes in

metabolite availability, indicating how these changes affect the HA-maximization objective. Under HA-maximising conditions, the strong positive shadow prices for upper glycolytic intermediates (G6P, F6P, FBP, G1P; ≈0.398) indicate that increased carbon entry through glycolysis would directly improve the achievable HA objective, consistent with the standard dual interpretation in LP-based FBA and its use for identifying objective-limiting metabolites.

Positive shadow prices maintained across downstream glycolysis (GAP/DHAP ≈0.199; 3PG/PEP/Pyr ≈0.165–0.167) support the same conclusion, such as carbon availability in central metabolism remains beneficial, but the marginal benefit declines as flux progresses toward energy-conversion nodes rather than immediate HA precursors. A progressive decline in marginal sensitivity typically occurs in constraint-based optimisation models where different metabolites contribute unequally to the objective.

Pentose phosphate pathway (PPP) intermediates show consistently positive sensitivities, with SH7P (≈0.464) and R5P/X5P (≈0.332) show high shadow prices. This supports the interpretation that PPP-mediated carbon redistribution (and associated redox/precursor balancing) is advantageous for HA formation, particularly because HA synthesis requires substantial sugar-nucleotide and nucleotide-related precursor supply.

The largest positive shadow prices occur in activated HA-precursor such as UDP-GlucNAc (≈0.534), GlucNAc-1P (≈0.665), and UDP-GlucUA (≈0.204) identifying sugar-nucleotide availability as the primary bottleneck for HA polymerisation. Recent HA production literature consistently emphasizes precursor supply and pathway-level flux engineering as key drivers for improving HA yield, aligning with your finding that sugar-nucleotide nodes carry the highest marginal value under HA optimisation.

As expected, HA[c] and HA[e] show unit shadow prices (1), which is consistent with HA export defining the objective, and therefore appearing as a direct marginal term in the dual interpretation. Nitrogen assimilation-related metabolites (NH_4^+, Gln, Ser) carrying positive shadow prices further indicate that amino-sugar formation and nucleotide metabolism incorporate an additional nutrient dependence for HA biosynthesis under the present constraints.

In contrast, negative shadow prices for TCA-associated intermediates (e.g., succinyl-CoA −2.11; OAA/α-KG ≈−0.163) and redox/respiration-linked terms (NAD^+/$NADP^+$,

O_2) indicate competition between respiratory/energy metabolism and HA-directed carbon allocation. Such negative dual values are consistent with the interpretation that increasing availability of these metabolites would shift the optimum toward flux states less favourable for HA production, reflecting a growth versus product-allocation trade-off frequently observed in constraint-based optimisation.

Overall, the shadow-price result provides model-level validation that HA maximisation is primarily constrained by (i) carbon routing into glycolysis/PPP and (ii) sugar-nucleotide precursor supply, while respiratory metabolism exerts an opposing pull on the optimum. This pattern is consistent with established dual-sensitivity theory in FBA and with recent work on improved sensitivity analysis and objective inference in constraint-based models.

Conclusion

This study presents a novel constraint based mathematical model to simulate gene knock out strategies in *Chlorella vulgaris* for HA production. The constructed model comprises of 216 reactions, 144 metabolites, and 318 genes. The gene knock-out of competing storage pathways (glycogen and cellulose) with enforced biomass constraints impacts the HA production rate. This validates the storage metabolism process as the primary bottleneck for carbon. The shadow-price analysis identified triglyceride cycle intermediates, primarily neutral lipid, as major competing sink for HA production. Overall, the model provides a mechanistic framework for the integrated control of nutrient supply, flux distribution across pathways, and gene-level regulation, with the aim of enhancing phototrophic HA production. It forms a quantitative basis for future strain engineering and process optimisation.

Declaration of competing interest

The authors declare that they have no known competing financial interests or personal relationships that could have appeared to influence the work reported in this paper.

Acknowledgement

The authors acknowledge the Department of Biotechnology and Medical Engineering of the National Institute of Technology Rourkela for providing the research facility.

References

Becker, S. A., Feist, A. M., Mo, M. L., Hannum, G., Palsson, B., & Herrgard, M. J. (2007). Quantitative prediction of cellular metabolism with constraint-based models: The COBRA Toolbox. *Nature Protocols*, *2*(3), 727–738. https://doi.org/10.1038/nprot.2007.99

Burgard, A. P., & Maranas, C. D. (2001). Probing the performance limits of the Escherichia coli metabolic network subject to gene additions or deletions. *Biotechnology and Bioengineering*, *74*(5), 364–375. https://doi.org/10.1002/bit.1127

Carter, E. L., Constantinidou, C., & Alam, M. T. (2024). Applications of genome-scale metabolic models to investigate microbial metabolic adaptations in response to genetic or environmental perturbations. In *Briefings in Bioinformatics* (Vol. 25, Issue 1). Oxford University Press. https://doi.org/10.1093/bib/bbad439

Case, A. E., & Atsumi, S. (2016). Cyanobacterial chemical production. In *Journal of Biotechnology* (Vol. 231, pp. 106–114). Elsevier B.V. https://doi.org/10.1016/j.jbiotec.2016.05.023

Feist, A. M., Zielinski, D. C., Orth, J. D., Schellenberger, J., Herrgard, M. J., & Palsson, B. O. (2010). Model-driven evaluation of the production potential for growth-coupled products of Escherichia coli. *Metabolic Engineering*, *12*(3), 173–186. https://doi.org/10.1016/j.ymben.2009.10.003

Grabowski, M., Gmyrek, D., Żurawska, M., & Trusek, A. (2025). Hyaluronic Acid: Production Strategies, Gel-Forming Properties, and Advances in Drug Delivery Systems. In *Gels* (Vol. 11, Issue 6). Multidisciplinary Digital Publishing Institute (MDPI). https://doi.org/10.3390/gels11060424

Griesemer, M., & Navid, A. (2023). Uses of Multi-Objective Flux Analysis for Optimization of Microbial Production of Secondary Metabolites. In *Microorganisms* (Vol. 11, Issue 9). Multidisciplinary Digital Publishing Institute (MDPI). https://doi.org/10.3390/microorganisms11092149

Heirendt, L., Arreckx, S., Pfau, T., Mendoza, S. N., Richelle, A., Heinken, A., Haraldsdóttir, H. S., Wachowiak, J., Keating, S. M., Vlasov, V., Magnusdóttir, S., Ng, C. Y., Preciat, G., Žagare, A., Chan, S. H. J., Aurich, M. K., Clancy, C. M., Modamio, J., Sauls, J. T., … Fleming, R. M. T. (2019). Creation and analysis of biochemical constraint-based models using the COBRA Toolbox v.3.0. *Nature Protocols*, *14*(3), 639–702. https://doi.org/10.1038/s41596-018-0098-2

Ho, J. K. (2000). Computing True Shadow Prices in Linear Programming. In *INFORMATICA* (Vol. 11, Issue 4).

Höper, R., Komkova, D., Zavřel, T., & Steuer, R. (2024). A quantitative description of light-limited cyanobacterial growth using flux balance analysis. *PLoS Computational Biology*, *20*(8 August). https://doi.org/10.1371/journal.pcbi.1012280

Kumar S, P., & Bhatt, N. P. (2025). ThermOptCobra: Thermodynamically optimal construction and analysis of metabolic networks for reliable phenotype predictions. *IScience*, *28*(8). https://doi.org/10.1016/j.isci.2025.113005

Lee, C. Y., Yang, S. F., Chen, H. C., Huang, J. Y., & Chang, C. K. (2025). The Effect of Hyaluronic Acid-contained Artificial Tear on Refractive Accuracy of Cataract Surgery in Dry Eye Population: A Retrospective Cohort Study. *In Vivo*, *39*(5), 2940–2949. https://doi.org/10.21873/invivo.14094

Li, K., Zhao, M., Li, Y., He, Y., Han, X., Ma, X., & Ma, F. (2024). Spatiotemporal Trends of the Carbon Footprint of Sugar Production in China. *Sustainable Production and Consumption*, *46*, 502–511. https://doi.org/10.1016/j.spc.2024.03.010

Lin, D. W., Khattar, S., & Chandrasekaran, S. (2025). Metabolic Objectives and Trade-Offs: Inference and Applications. In *Metabolites* (Vol. 15, Issue 2). Multidisciplinary Digital Publishing Institute (MDPI). https://doi.org/10.3390/metabo15020101

Liu, Z. Y., & Yu, X. Z. (2025). Engineering Bacillus subtilis for high-value bioproduction: recent advances and applications. In *Microbial Cell Factories* (Vol. 24, Issue 1). BioMed Central Ltd. https://doi.org/10.1186/s12934-025-02818-6

Mahadevan, R., & Schilling, C. H. (2003). The effects of alternate optimal solutions in constraint-based genome-scale metabolic models. *Metabolic Engineering*, *5*(4), 264–276. https://doi.org/10.1016/j.ymben.2003.09.002

Marler, R. T., & Arora, J. S. (2010). The weighted sum method for multi-objective optimization: New insights. *Structural and Multidisciplinary Optimization*, *41*(6), 853–862. https://doi.org/10.1007/s00158-009-0460-7

Mori, M., Hwa, T., Martin, O. C., De Martino, A., & Marinari, E. (2016). Constrained Allocation Flux Balance Analysis. *PLoS Computational Biology*, *12*(6). https://doi.org/10.1371/journal.pcbi.1004913

Muthuraj, M., Palabhanvi, B., Misra, S., Kumar, V., Sivalingavasu, K., & Das, D. (2013). Flux balance analysis of Chlorella sp. FC2 IITG under photoautotrophic and heterotrophic growth conditions. *Photosynthesis Research*, *118*(1–2), 167–179. https://doi.org/10.1007/s11120-013-9943-x

Orth, J. D., Thiele, I., & Palsson, B. O. (2010). What is flux balance analysis? In *Nature Biotechnology* (Vol. 28, Issue 3, pp. 245–248). https://doi.org/10.1038/nbt.1614

Palenčárová, K., Köszagová, R., & Nahálka, J. (2025a). Hyaluronic Acid and Its Synthases—Current Knowledge. In *International Journal of Molecular Sciences* (Vol. 26, Issue 15). Multidisciplinary Digital Publishing Institute (MDPI). https://doi.org/10.3390/ijms26157028

Palenčárová, K., Köszagová, R., & Nahálka, J. (2025b). Hyaluronic Acid and Its Synthases—Current Knowledge. *International Journal of Molecular Sciences*, *26*(15), 7028. https://doi.org/10.3390/ijms26157028

Saadh, M. J., Ahmed, H. H., Kareem, R. A., Bishoyi, A. K., Roopashree, R., Shit, D., Arya, R., Joshi, K. K., Sameer, H. N., Yaseen, A., Athab, Z. H., Adil, M., Narmani, A., & Farhood, B. (2025). Recent advances of hyaluronic acid-based materials in drug delivery systems and regenerative medicine: A review. In *Archiv der Pharmazie* (Vol. 358, Issue 3). John Wiley and Sons Inc. https://doi.org/10.1002/ardp.202400903

Salih, A. R. C., Farooqi, H. M. U., Amin, H., Karn, P. R., Meghani, N., & Nagendran, S. (2024). Hyaluronic acid: comprehensive review of a multifunctional biopolymer. *Future Journal of Pharmaceutical Sciences*, *10*(1). https://doi.org/10.1186/s43094-024-00636-y

Scott, W. T., Benito-Vaquerizo, S., Zimmermann, J., Bajić, D., Heinken, A., Suarez-Diez, M., & Schaap, P. J. (2023). A structured evaluation of genome-scale constraint-based modeling tools for microbial consortia. *PLoS Computational Biology*, *19*(8 August). https://doi.org/10.1371/journal.pcbi.1011363

Shang, L., Li, M., Xu, A., & Zhuo, F. (2024). Recent applications and molecular mechanisms of hyaluronic acid in skin aging and wound healing. *Medicine in Novel Technology and Devices*, *23*. https://doi.org/10.1016/j.medntd.2024.100320

Son, J., Lee, H. J., & Woo, H. M. (2025). CRISPRi-assisted metabolic engineering of cyanobacteria for photosynthetic hyaluronic acid from CO2. *Journal of Biological Engineering*, *19*(1). https://doi.org/10.1186/s13036-025-00494-z

Song, H. S., Ahamed, F., Lee, J. Y., Henry, C. S., Edirisinghe, J. N., Nelson, W. C., Chen, X., Moulton, J. D., & Scheibe, T. D. (2025). Coupling flux balance analysis with reactive transport modeling through machine learning for rapid and stable simulation of microbial metabolic switching. *Scientific Reports*, *15*(1). https://doi.org/10.1038/s41598-025-89997-9

Sundaram, M. K., Balavigneswaran, C. K., Saravanakumar, I., Jayaraman, G., & Muthuvijayan, V. (2025). Recombinant hyaluronic acid-incorporated self-healing injectable hydrogels for cartilage tissue engineering: a case study on effects of molecular weight. *Journal of Materials Chemistry B*, *13*(31), 9589–9606. https://doi.org/10.1039/d5tb00248f

Wei, M., Huang, Y., Zhu, J., Qiao, Y., Xiao, N., Jin, M., Gao, H., Huang, Y., Hu, X., & Li, O. (2024). Advances in hyaluronic acid production: Biosynthesis and genetic engineering strategies based on Streptococcus — A review. In *International Journal of Biological Macromolecules* (Vol. 270). Elsevier B.V. https://doi.org/10.1016/j.ijbiomac.2024.132334

Wróbel-Jędrzejewska, M., Przybysz, Ł., & Włodarczyk, E. (2024). Carbon footprint analysis of sugar production in Poland. *Food and Bioproducts Processing*, *148*, 88–94. https://doi.org/10.1016/j.fbp.2024.08.014

Yang, Y., Tang, S., & Chen, J. P. (2024). Carbon capture and utilization by algae with high concentration CO2 or bicarbonate as carbon source. In *Science of the Total Environment* (Vol. 918). Elsevier B.V. https://doi.org/10.1016/j.scitotenv.2024.170325

Yu, X., Guo, W., Hu, Z., Li, P., Zhang, Z., Cheng, J., Song, C., & Ye, Q. (2023). Flue gas CO2 supply methods for microalgae utilization: A review. In *Clean Energy Science and Technology* (Vol. 1, Issue 2). Universe Scientific Publishing Pte. Ltd. https://doi.org/10.18686/cest.v1i2.78

Zhang, L., Toscano Selão, T., Nixon, P. J., & Norling, B. (2019). Photosynthetic conversion of CO2 to hyaluronic acid by engineered strains of the cyanobacterium Synechococcus sp. PCC 7002. *Algal Research*, *44*. https://doi.org/10.1016/j.algal.2019.101702

Zhang, Y., Dong, J., Xu, G., Han, R., Zhou, J., & Ni, Y. (2023). Efficient production of hyaluronic acid by Streptococcus zooepidemicus using two-stage semi-continuous fermentation. *Bioresource Technology*, *377*. https://doi.org/10.1016/j.biortech.2023.128896

Zuñiga, C., Li, C. T., Huelsman, T., Levering, J., Zielinski, D. C., McConnell, B. O., Long, C. P., Knoshaug, E. P., Guarnieri, M. T., Antoniewicz, M. R., Betenbaugh, M. J., & Zengler, K. (2016). Genome-scale metabolic model for the green alga chlorella vulgaris UTEX 395 accurately predicts phenotypes under autotrophic, heterotrophic, and mixotrophic growth conditions. *Plant Physiology*, *172*(1), 589–602. https://doi.org/10.1104/pp.16.00593